

Effect of mechanical activation on the thermoelectric properties of $\text{Sr}_{1-x}\text{Sm}_x\text{TiO}_3$ ceramics

Yu.S. Orlov^{a,b,*}, S.N. Vereshchagin^c, S.V. Novikov^d, A.T. Burkov^d, A.A. Borus^a, M.V. Sitnikov^b, L.A. Solov'yov^c, M.N. Volochaev^a, V.A. Dudnikov^{a,b}

^a Kirensky Institute of Physics, Krasnoyarsk Scientific Center, Siberian Branch, Russian Academy of Sciences, Krasnoyarsk, 660036, Russia

^b Siberian Federal University, Krasnoyarsk, 660041, Russia

^c Institute of Chemistry and Chemical Technology, Krasnoyarsk Scientific Center, Siberian Branch, Russian Academy of Sciences, Krasnoyarsk, 660036, Russia

^d Ioffe Institute, St. Petersburg, 194021, Russia

ARTICLE INFO

Keywords:

Strontium titanate solid solutions
Thermoelectric oxide materials
Mechanochemical activation

ABSTRACT

The $\text{Sr}_{1-x}\text{Sm}_x\text{TiO}_3$ ($x = 0.025, 0.05, 0.075, 0.1, 0.2$) strontium titanate solid solutions were prepared from oxides and carbonates using a conventional ceramic technology based on the mechanochemical activation. The electrical conductivity and Seebeck coefficient of the synthesized compounds were measured in the temperature range from 300 to 800 K. We found that the properties of the samples significantly depend on the preliminary mechanochemical activation. The thermoelectric power factor attains maximum value in the hydrogen reduced samples with concentration of $x = 0.05$ and 0.075 obtained from nanoparticles: $5.5 \mu\text{W}/(\text{cm} \cdot \text{K}^2)$ for $\text{Sr}_{0.95}\text{Sm}_{0.05}\text{TiO}_3$ (580 K) and $4.10 \mu\text{W}/(\text{cm} \cdot \text{K}^2)$ for $\text{Sr}_{0.925}\text{Sm}_{0.075}\text{TiO}_3$ (650 K). An increase in the annealing temperature of mechanically activated samples leads to an even greater increase in electrical conductivity and power factor: $9.2 \mu\text{W}/(\text{cm} \cdot \text{K}^2)$ for $\text{Sr}_{0.925}\text{Sm}_{0.075}\text{TiO}_3$ (650 K).

1. Introduction

Recently the problems of environment energy pollution and waste-heat utilization have become increasingly acute. Thermoelectric energy converters can transform the low-potential heat energy into useful electricity, thus providing a solution for waste-heat utilization. To make this technology economically viable it is necessary to increase the conversion efficiency of the thermoelectric converters and to decrease their cost. Therefore, improving the characteristics of available thermoelectric materials and searching for new high-thermoelectric-figure-of-merit compounds are urgent tasks. Considerable attention is paid, along with the classical thermoelectrics, to the oxide materials with a perovskite structure [1], which are less toxic, cheaper, and, sometimes, much more stable in an oxidizing atmosphere.

The main characteristic of thermoelectric materials is the dimensionless figure of merit $ZT = S^2\sigma/\kappa$ [2–4], where S is the Seebeck coefficient, σ is the electrical conductivity, κ is the total thermal conductivity, and T is the absolute temperature. For all materials used in commercial production of thermoelectric devices $ZT \leq 1$. The efficiency of thermoelectric converters based on such materials do not exceed 10%.

The implementation of an advanced thermoelectric converter requires n - and p -type-conductivity materials with the higher ZT values and with similar thermal expansion coefficients.

Promising n -type-conductivity thermoelectric materials are strontium titanate-based compounds [5]. The parent composition SrTiO_3 is a virtual ferroelectric, which is a typical ABO_3 cubic perovskite (sp. gr. $Pm\bar{3}m$) with a lattice parameter of $a = 3.904 \text{ \AA}$ [6]. The properties of the SrTiO_3 compound depend, to a great extent, on doping with different elements and on synthesis techniques, which cause various microstructure modulations [7–9]. To improve the thermoelectric properties of strontium titanate, stoichiometric substitution in the A and B sites [10–15] and the creation of a certain degree of nonstoichiometry in these sites [16–19] were used.

An increase in the content of a rare-earth metal (REM) as a dopant in the A site leads to an increase in the electrical conductivity and a decrease in the absolute value of the Seebeck coefficient. As was shown in [20], doping with large REM ions leads to the higher power factor, while doping with smaller REM ions reduces the thermal conductivity.

Despite a great number of works devoted to the replacement of strontium by REMs, we have not come across any systematic studies on

* Corresponding author. Kirensky Institute of Physics KSC SB RAS, 660036, Krasnoyarsk, Russia.,
E-mail address: orlov@iph.krasn.ru (Yu.S. Orlov).

<https://doi.org/10.1016/j.ceramint.2021.07.060>

Received 6 April 2021; Received in revised form 20 June 2021; Accepted 6 July 2021

Available online 7 July 2021

0272-8842/© 2021 Elsevier Ltd and Techna Group S.r.l. All rights reserved.

the effect of substitution of samarium ions for strontium ones. Here, we investigate the properties of the $\text{Sr}_{1-x}\text{Sm}_x\text{TiO}_3$ solid solutions in the temperature range of 300–800 K as a function of the doping level at $x = 0.02, 0.05, 0.075, 0.1, \text{ and } 0.2$ and the preliminary mechanochemical activation.

The thermoelectric efficiency of materials can be improved by using nanocrystalline structures. This is contributed by three mechanisms: (1) additional phonon scattering by nanograin boundaries, (2) electron tunneling between nanostructure elements, and (3) carrier energy filtering as a consequence of the presence of potential barriers between nanograins. If the grain size in samples is less than tens of nanometers and the separation between grains is on the order of a few nanometers, the carrier free path exceeds the grain size and the lattice component of thermal conductivity decreases more significantly than the electrical conductivity of the material. A decrease in grain size in nanostructures can be accompanied by an increase in Seebeck coefficient owing to carrier energy filtering [21].

The purpose of this work is to find out how thermoelectric parameters of SrTiO_3 samples doped with Sm ions depend on preparation conditions of the starting powder, produced by grinding an ingot to various size fractions. There is currently considerable attention paid to activation by grinding as a process for the chemical synthesis of solid solutions at lower temperatures. It is accepted to call the treatment of powder materials in planetary spherical mills and in other devices with high energy mechanical actions (vibration, jetmills, devices of intense plastic deformation, etc.) mechanical activation. As a result of mechanical action, the grinding of fragile phases and the repeated plastic deformation of plastic phases take place; crystal structure defects and residual stresses are accumulated. It results in modifying the chemical and physical properties of the processed powders and the materials obtained from them.

2. Experimental

The samples were synthesized by a conventional ceramic technology from stoichiometric amounts of TiO_2 (99.7%, metals basis, Alfa Aesar) and Sm_2O_3 (99.99%, REO, Alfa Aesar) oxides and SrCO_3 carbonate (99.99%, Alfa Aesar). At the first stage, the initial powders were thoroughly mixed in an agate mortar using ethanol and annealed in air at 1573 K in a corundum crucible for 24 h. The resulting mixture was ground. A part of the mixture was pressed in 2-mm-thick disk tablets 20 mm in diameter, annealed in air at 1573 K for 6 h, and cooled with furnace to room temperature at a rate of $2^\circ/\text{min}$ (hereinafter, sample STO-1). Another part of the annealed mixture was subjected to the mechanochemical activation in octane in a planetary micromill (Pulverisette 7 premium line Fritsch GmbH, Germany) using a milling pot made of zirconium dioxide (96.2% ZrO_2) and ZrO_2 balls 3 mm in diameter. The total grinding time was 80 min at 1100 rpm (hereinafter, sample STO-2). After crushing and evaporation of the obtained mixture, tablets were pressed and sintered similarly to samples STO-1. To study the thermoelectric properties of samples STO-1 and STO-2, bars $5 \times 13 \times 2$ mm in size were used, which were preliminarily reduced in a 5% H_2 -He mixture flow according to the procedure that included heating to 1573 K at a rate of $6^\circ/\text{min}$, holding at 1573 K for 1 h, and cooling in a furnace in the flow to room temperature. It should be noted that the synthesis and reduction temperatures were much lower than conventionally used [23].

The powder X-ray diffraction (PXRD) data were obtained on a PANalytical X'Pert PRO diffractometer equipped with a PIXcel solid-state detector (CoK_α radiation) in the 2θ range of $(10\text{--}150)^\circ$. The powder samples were prepared by grinding of the bars in octane in an agate mortar and packed in a flat sample holder for the PXRD measurements in the Bragg–Brentano geometry. The full-profile PXRD refinement was performed by the derivative difference minimization (DDM) method [24].

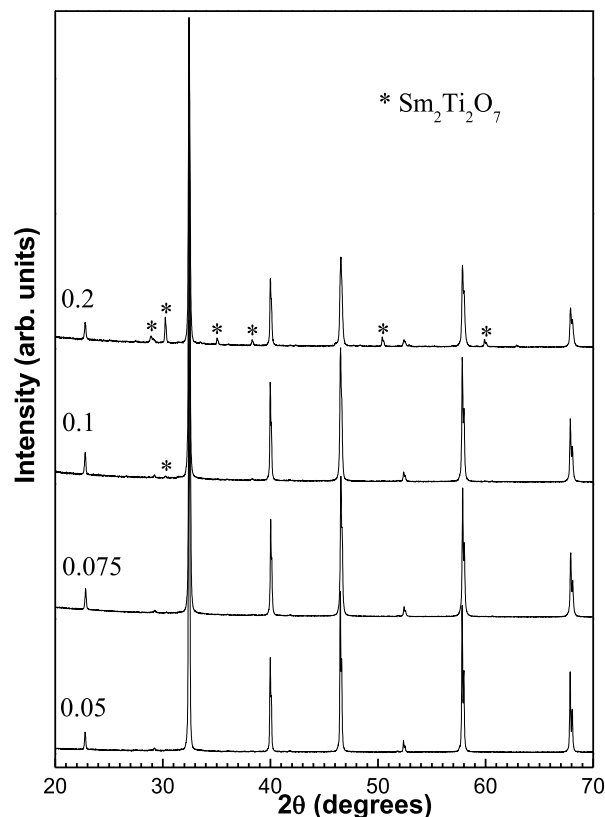


Fig. 1. PXRD patterns of the $\text{Sr}_{1-x}\text{Sm}_x\text{TiO}_3$ samples with different Sm contents at $x = 0.05, 0.075, 0.1, \text{ and } 0.2$. The $\text{Sm}_2\text{Ti}_2\text{O}_7$ peaks are marked by the asterisk.

The simultaneous thermal analysis (STA) experiments were performed on a TG-DSC NETZSCH STA 449C analyzer equipped with an Aeolos QMS 403C mass spectrometer. The thermogravimetry and differential scanning calorimetry (TG-DSC) measurements were performed in the dynamic 20% O_2 -Ar atmosphere at a pressure of $P = 101$ kPa in open platinum crucibles; for a run, a monolithic sample about $2 \times 2 \times 1$ mm in size was used.

The surface morphology and the degree of crystallinity of the samples were visualized on a Hitachi TM4000 Plus scanning electron microscope (SEM). The electron microscopy investigations were carried out on the equipment of the Krasnoyarsk Regional Center for Collective Use of the Krasnoyarsk Scientific Center, Siberian Branch of the Russian Academy of Sciences.

The temperature dependences of the Seebeck coefficient and electrical resistivity were obtained with original experimental setups at the Kirensky Institute of Physics, Siberian Branch of the Russian Academy of Sciences (Krasnoyarsk) and at the Ioffe Institute (St. Petersburg) [25, 26]. The measurement error is for electrical resistance - 2%, for measurements of the Seebeck coefficient - 5%.

3. Results and discussion

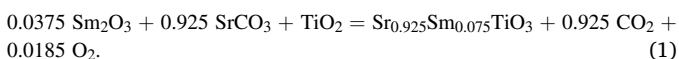
The STA study of the thermochemical transformation of the charge on samples STO-1 and STO-2 showed that the formation of a perovskite occurs at temperatures of >1300 K (STO-1) and >1215 K (STO-2) and, according to the XRD data (Supplementary materials), during the preliminary mechanochemical activation a perovskite did not form. A mass variation of $\Delta m = 17.98\%$ per dry charge upon heating, by the example, of the $\text{Sr}_{0.925}\text{Sm}_{0.075}\text{TiO}_3$ composition (Fig. S2, Table S1) is consistent

Table 1

Tetragonal ($I4/mcm$) crystal lattice parameters, theoretical density and experimental porosity of the $Sr_{1-x}Sm_xTiO_{3-\delta}$ samples.

Sample	x	a , Å	c , Å	ρ_{theor} , g/cm ³	porosity, %
STO-1	0.05	5.5209 (2)	7.8107 (3)	5.21	31.2
STO-1	0.075	5.5186 (1)	7.8107 (2)	5.27	33.5
STO-1	0.1	5.5170 (1)	7.8113 (2)	5.30	33.8
STO-1	0.2	5.5146 (2)	7.8123 (3)	5.48	39.5
STO-2	0.075	5.5201 (1)	7.8209 (3)	5.25	14.6

with the theoretical value of $\Delta m = 17.99\%$ for the perovskite formation reaction



Therefore, the compositions of the initial perovskites before hydrogen reduction can be considered close to the stoichiometric $Sr_{1-x}Sm_xTiO_{3-\delta}$ compositions. The main results of the preliminary mechanochemical activation were a decrease in the strontium carbonate decomposition temperature and a pronounced decrease in the temperature of the exothermic process related to the formation of a perovskite structure (Fig. S2, Supplementary materials).

The $Sr_{1-x}Sm_xTiO_{3-\delta}$ samples reduced in the 5% H_2 -He mixture flow were stable in air up to 700 K; at higher temperatures they oxidized by oxygen with evident mass gain (Fig. S3): a value of $\Delta m = 0.15\%$ observed for the $Sr_{0.925}Sm_{0.075}TiO_{3-\delta}$ sample corresponded to $\delta = 0.0187$.

The XRD data show (Fig. 1) that the $Sr_{1-x}Sm_xTiO_3$ (STO-1, $x = 0.025$,

0.05, and 0.075) samples are perovskites with the tetragonal symmetry (sp. gr. $I4/mcm$); no foreign phases were observed. As the samarium content increases (at $x = 0.1$ and 0.2), an additional pyrochlore-type phase ($Sm_2Ti_2O_7$) arises and its content increases with x . The increase in the content of the secondary phase with increasing x is consistent with the data reported in [20]. The crystal lattice parameters at $T = 298$ K for different x values are given in Table 1.

The STO-1 lattice parameters are much smaller than the STO-2 ones. For example, for $Sr_{0.925}Sm_{0.075}TiO_{3-\delta}$ in STO-1, we have $a = b = 5.5186$ (1) and $c = 7.8107$ (2), while for STO-2, $a = b = 5.5201$ (1) and $c = 7.8209$ (3). In addition, the STO-2 peaks are much broader due to the smaller crystallite size and stronger lattice microdistortions (Fig. S1).

The evaluation of the samples porosity and density showed that the theoretical samples density, calculated from the X-ray diffraction data, increases with an increase in the samarium content, which is probably due to the smaller ionic radius of samarium ions in comparison with the ionic radius of strontium ions (Table 1). Nevertheless, the experimental samples density decreases with increasing x . For samples subjected to mechanical activation (STO-2), the density significantly increases in comparison with the STO-1 samples (Table 1). The decrease in the samples porosity is clearly seen from the data of scanning electron microscopy (see below).

Fig. 2 shows temperature dependences of the resistivity ρ , electrical conductivity σ , Seebeck coefficient S , and thermoelectric power factor $P = S^2/\rho$ for the $Sr_{1-x}Sm_xTiO_{3-\delta}$ (STO-1) samples. In contrast to the results obtained in [8,11], where the $Sr_{1-x}Nd_xTiO_3$ ($x = 0.025, 0.05, 0.1$) and $Sr_{1-x}Ln_xTiO_3$ ($Ln = La, Sm, Gd, Dy, Y$) samples exhibited the metal-type conductivity at high (above 450 K) temperatures, in our study, all samples STO-1 were characterized by the semiconductor-type

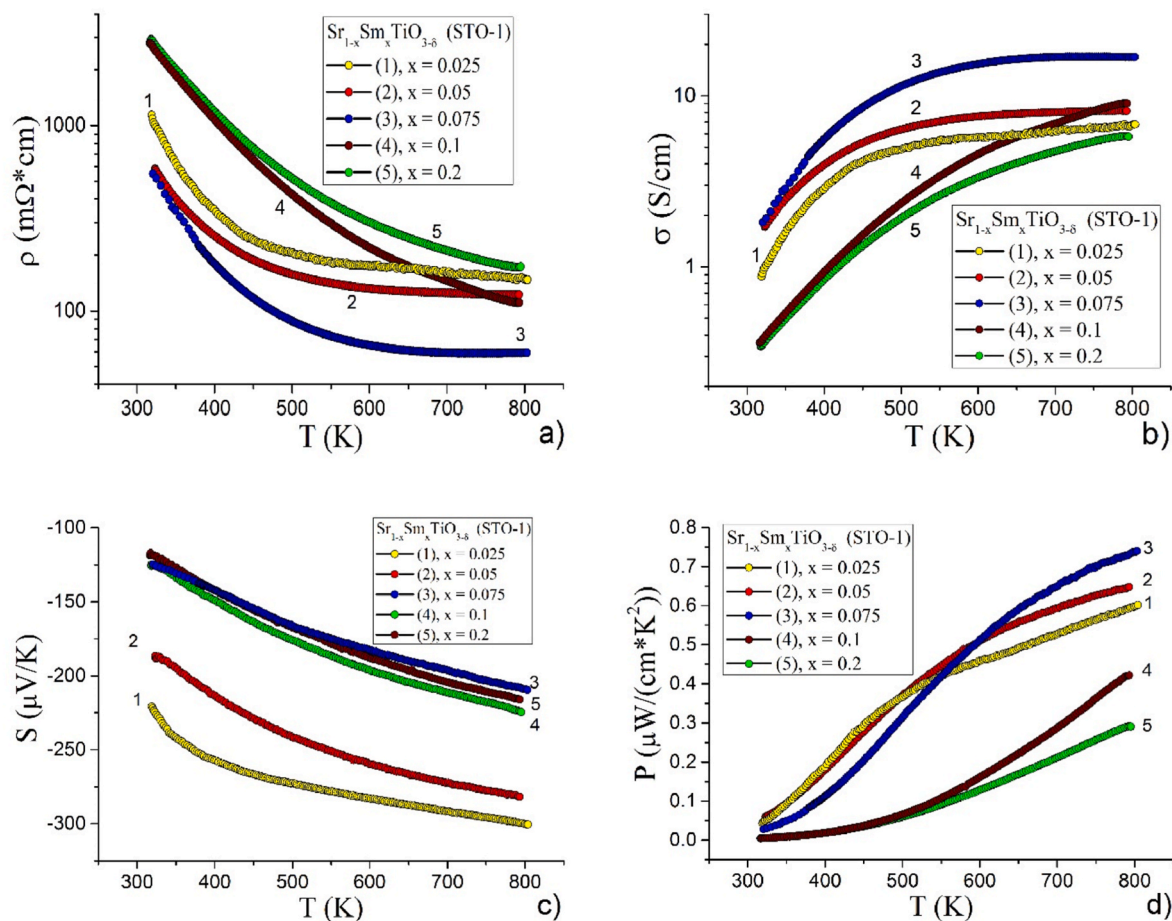


Fig. 2. Temperature dependences of (a) the electrical resistivity, (b) electrical conductivity, (c) Seebeck coefficient, and (d) thermoelectric power factor for the $Sr_{1-x}Sm_xTiO_3$ (STO-1) samples with different doping levels.

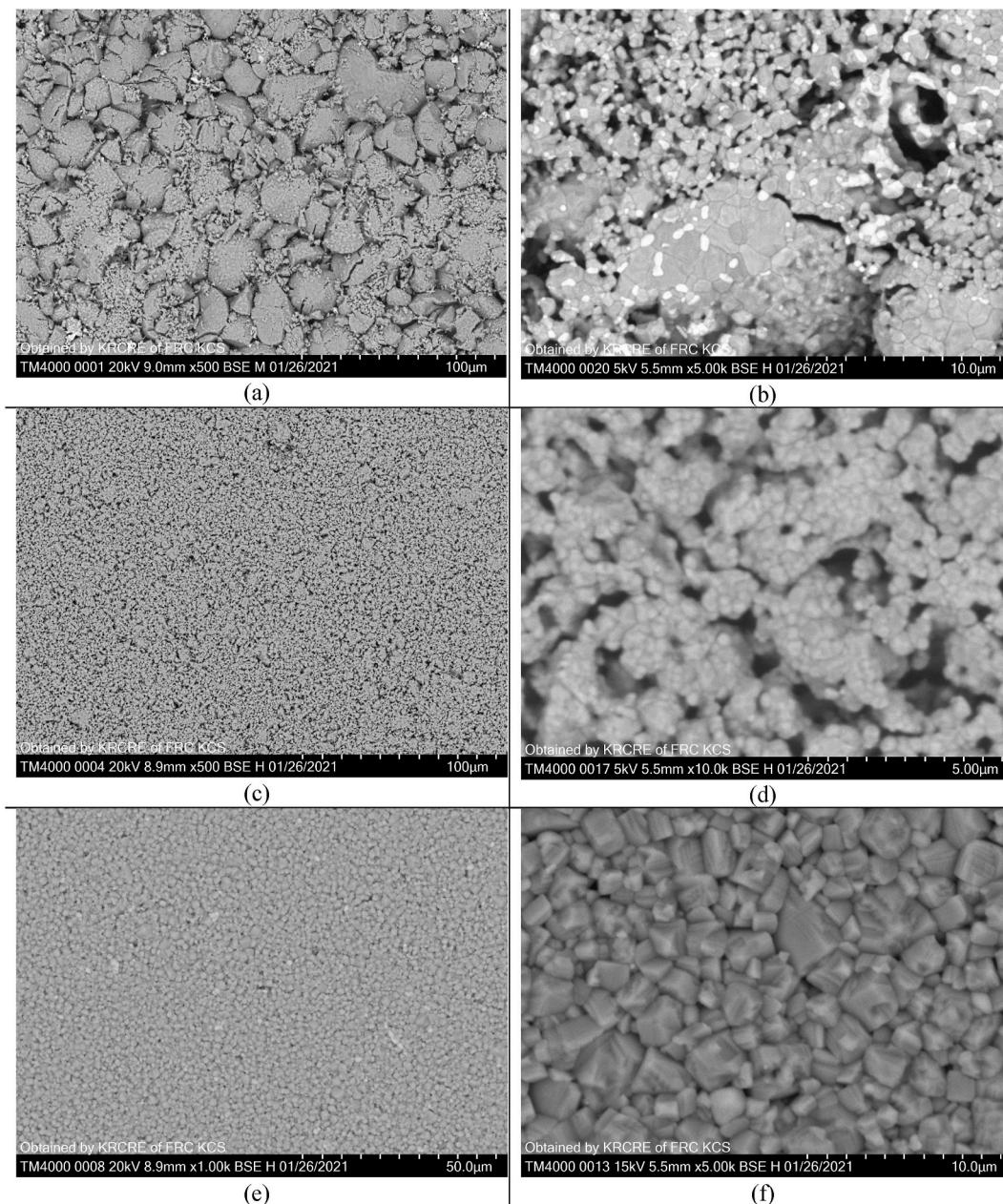


Fig. 3. SEM images of the surface of the $\text{Sr}_{0.95}\text{Sm}_{0.05}\text{TiO}_3$ samples without mechanochemical activation (STO-1, (a, b)) and additionally crushed in a micromill for 80 min in total at 800 rpm (STO-2, (c, d)) and 1100 rpm (STO-2, (e, f)).

conductivity over the entire temperature range of up to 800 K ($d\rho/dT < 0$) (Fig. 2a). The $\sigma(T)$ curves for the samples with $x = 0.025, 0.05,$ and 0.075 are essentially different from the $\sigma(T)$ curves for $x = 0.1$ and 0.2 (Fig. 2b). In particular, the latter were characterized by the monotonically increasing electrical conductivity, while the former demonstrated a pronounced trend to reaching a plateau. The maximum absolute values of the Seebeck coefficient ($|S| = 300 \mu\text{V}/\text{K}$ at 800 K) were obtained for the samples with the minimum samarium content ($x = 0.025$) (Fig. 2c). An increase in the samarium content in the sample leads to a decrease in the absolute value of the Seebeck coefficient and to an increase in the electrical conductivity, which is consistent with data for $\text{Sr}_{1-x}\text{Nd}_x\text{TiO}_3$ [8], $\text{Sr}_{1-x}\text{R}_x\text{TiO}_3$ ($x = 0.05\text{--}0.2, \text{R} = \text{Y, La, Sm, Gd, Dy}$) [11] and $\text{Sr}_{1-x}\text{Pr}_x\text{TiO}_3$ [9].

An increase in the samarium content in samples STO-1 from $x = 0.025$ to 0.075 leads to a decrease in the resistivity and, consequently, to an increase in the electrical conductivity, which is related to an increase in the carrier density. However, a further increase in the samarium

content deteriorates the electrical conductivity, which can be caused by either the appearance of a pyrochlore-type secondary phase [18] or by the formation of extended defects containing excess oxygen [9]. The Seebeck coefficient for the samples with $x \geq 0.075$ are almost the same. A gradual increase in the electrical conductivity and the absolute value of the Seebeck coefficient with temperature leads to the monotonic growth of the thermoelectric power factor P over the entire investigated temperature range (300–800 K) (Fig. 2d).

The mechanical activation in a micromill significantly changes both the morphology of the samples and their thermoelectric properties. During the activation, the initial powder particle size (before sintering the tablets) decreases by a factor of more than 20 and is 2–5 μm for STO-1 and 50–100 nm for STO-2. Fig. 3 (see Fig. S4 and Fig. S5 for additional details) shows SEM images of the surfaces of the synthesized $\text{Sr}_{0.95}\text{Sm}_{0.05}\text{TiO}_3$ tablet samples without mechanochemical activation (STO-1, (a, b)), crushed in micromill for 80 min at 800 rpm (c, d), and for 80 min at 1100 rpm (STO-2, (e, f)). It can be clearly seen in Fig. 3 that the

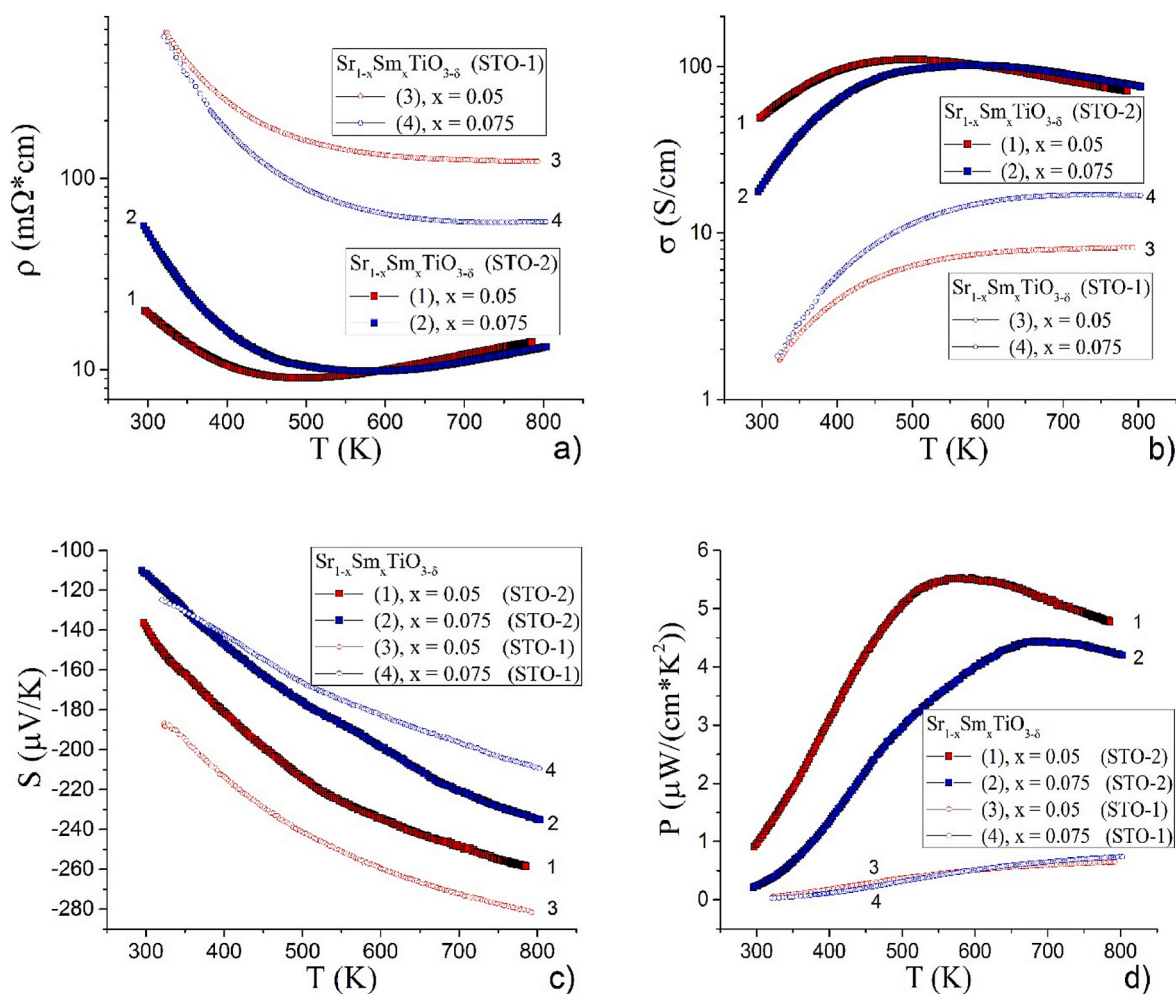


Fig. 4. Temperature dependences of (a) the electrical resistivity, (b) electrical conductivity, (c) Seebeck coefficient, and (d) thermoelectric power factor for the $\text{Sr}_{1-x}\text{Sm}_x\text{TiO}_{3-\delta}$ samples (STO-2) with different doping levels (curves 1 and 2). For convenience of comparison, the results of similar measurements for the STO-1 samples are also shown by curves 3 and 4.

morphology of the samples changes with the degree of their mechanical activation. Samples STO-2 are characterized by dense packing, low porosity, and a larger grain size. As the x value increases, the sintering capacity of the samples decreases, which is consistent with the SEM data on the $\text{Sr}_{1-x}\text{Pr}_x\text{TiO}_3$ samples reported in [9].

In an inert atmosphere, the samples are stable over the entire investigated temperature range. Heating in an oxidizing atmosphere (air) leads to the irreversible behavior of the samples; at temperatures around 600 K, the electrical resistance abruptly increases, leading to the drop of the power factor to almost zero values.

As was noted in [18], the introduction of the pyrochlore-type secondary phase does not improve the thermoelectric properties of SrTiO_3 ceramics. Therefore, further investigations of the properties of $\text{Sr}_{1-x}\text{Sm}_x\text{TiO}_3$ were mainly focused on the samples with $x = 0.05$ and 0.075.

Fig. 4 shows temperature dependences of the electrical resistivity, electrical conductivity, Seebeck coefficient, and thermoelectric power factor for the $\text{Sr}_{1-x}\text{Sm}_x\text{TiO}_{3-\delta}$ (STO-2, $x = 0.05, 0.075$) samples subjected to the mechanical activation (curves 1 and 2). For convenience of comparison, the results of similar measurements for the STO-1 samples are also shown in Fig. 4 by curves 3 and 4. The electrical resistivity curves of samples STO-2 are essentially different. In the temperature ranges of 400–500 K for $\text{Sr}_{0.95}\text{Sm}_{0.05}\text{TiO}_{3-\delta}$ and 500–600 K for $\text{Sr}_{0.925}\text{Sm}_{0.075}\text{TiO}_{3-\delta}$, the conductivity changes from semiconductor-to metal-type. The Seebeck coefficient, in contrast to the electrical

conductivity, weakly depends on the crystallite size and does not significantly differ from that for samples STO-1.

In contrast to the power factor of samples STO-1, the $P(T)$ dependences for samples STO-2 have maxima. At the temperatures corresponding to the maxima in the temperature dependences of the power factor, the absolute values of the electrical conductivity for STO-2 are almost an order of magnitude higher than for STO-1.

It is interesting to see that there is minimal change in Seebeck coefficient (Fig. 4c) of STO-1 and STO-2 samples despite there being a significant change in the electronic conductivity (Fig. 4b), which could be more related to the microstructure of the processed materials. The Seebeck coefficient is a property highly dependent on intrinsic electronic band structure, while the electronic conductivity can be affected much more by extrinsic factors such as ceramic microstructure, pores and grain boundaries. The electrical conductivity is directly proportional to carrier concentration $n\sigma = ne\mu$, where μ is the carrier mobility and on the other hand the Seebeck coefficient is inversely proportional to carrier concentration $S = \frac{8\pi^2 k_B^2}{3eh^2} m^* T \left(\frac{\pi}{3n}\right)^{2/3}$, where k_B stands for Boltzmann constant, e for electron charge, h refers to Planck's constant, m^* accounts for the effective mass of the carrier, T is the absolute temperature. The carrier concentration in all the samples is the same since the doping level is the same for all the samples. That why we do not see any significant changes in Seebeck coefficient contrary to the conductivity of STO-1 and STO-2 samples. Microstructure changes caused by mechanoactivation are significantly affecting carrier mobility. From Fig. 3 (a,

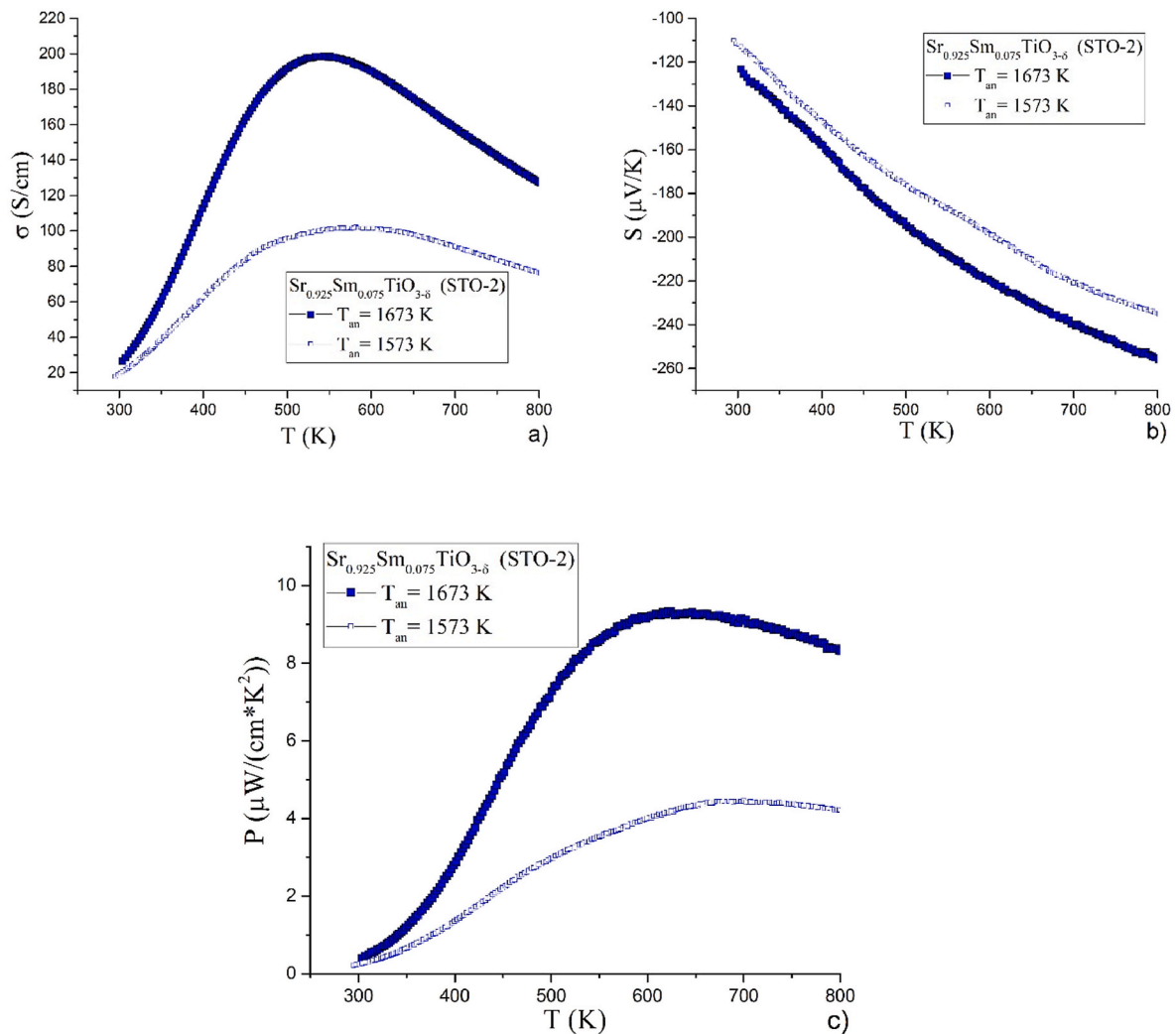


Fig. 5. Temperature dependences of (a) electrical conductivity, (b) Seebeck coefficient, and (c) thermoelectric power factor for the mechanically activated Sr_{0.925}Sm_{0.075}TiO_{3-δ} sample annealed at a higher temperature $T_{\text{an}} = 1673$ K (filled squares). For convenience of comparison, the results of similar measurements for the Sr_{0.925}Sm_{0.075}TiO_{3-δ} sample annealed at $T_{\text{an}} = 1573$ K from Fig. 4 are also shown by empty squares.

b) and (e, f) it can be seen that the unactivated Sr_{0.95}Sm_{0.05}CoO_{3-δ} sample has a more complex hierarchical multiscale structure. Ceramic grains ranging in size from 0.5 to 2 μm form larger agglomerates from 5 to 50 μm in size. In turn, the ceramic grains themselves can be formed from conjugated crystallites with intracrystalline disorder caused by the random arrangement of Sr and Sm ions in the lattice. From Fig. 3 (a) and (b) we can see that the ceramic grains inside the agglomerates are tightly conjugated to each other, and the agglomerates themselves are rather poorly connected to each other, forming cavities and voids between themselves. In the case of mechanically activated samples (Fig. 3 (e, f)), the formation of agglomerates is not observed. Instead, ceramic grains ranging in size from 1 to 5 μm form a fairly dense structure. Such a significant difference in the morphology and microstructure of the samples leads to a strong difference in their electrical conductivity due to carrier scattering, while maintaining approximately the same Seebeck coefficient. As a result, we observe a significant increase in the power factor of STO-1 samples in comparison with STO-2.

To fabricate a thermoelectric module based on oxide materials, the zT of n -type oxides should be improved to the level of p -type materials. Strontium titanate is a well-known n -type thermoelectric material with a cubic perovskite crystal structure. It has been reported that high zT has been achieved for La-doped SrTiO₃ by creating a defective perovskite lattice containing A and O-site vacancies with mixed valence Ti³⁺ and Ti⁴⁺ on the B-sites [27,28]. The effects of spark plasma sintering (SPS)

time on thermoelectric properties of La-doped SrTiO₃ have also been reported [29]. In another report, La-doped SrTiO₃ nanostructured bulk has been synthesized by SPS from chemically synthesized colloidal nanocrystals [30]. It has been reported that the addition of nanosized Ag metal particles in Sr_{0.9}La_{0.1}TiO₃ causes an increase in the carrier concentration and that the electrical connection is built into Ag particle between the grains. They improve the electrical conductivity and reduce the thermal conductivity [31]. The effect of nanoscale porosity on the thermoelectric properties of La-doped SrTiO₃ bulks has been published in [32]. It is reported that the nanoscale porosity suppresses the thermal conductivity and significantly enhances the Seebeck coefficient by the phonon and carrier scattering respectively. The results of recent advances in improving thermoelectric properties of SrTiO₃-based systems can be found in the review [33].

The effect of mechanoactivation on the thermoelectric properties of REM-doped SrTiO₃ bulks has not been published. Here, it is reported for the first time that mechanical activation in a Sm-doped SrTiO₃ bulk sample has a significant impact on its thermoelectric properties. Mechanical activation significantly enhances the electrical conductivity, leaving the Seebeck coefficient practically unchanged. Therefore, there is an overall improvement in the power factor of Sm-doped SrTiO₃. The obtained power factor values are comparable with the best results achieved for REM-doped SrTiO₃ thermoelectrics [33]. Thus, this allows us to consider mechanical activation as another way to improve the

thermoelectric properties of SrTiO₃-based materials.

At the conclusion of this section in Fig. 5, we plotted the results of measurements of thermoelectric performance for mechanically activated Sr_{0.925}Sm_{0.075}TiO_{3-δ} solid solution annealed at a higher temperature $T_{\text{an}} = 1673$ K (filled squares). The porosity of such sample is 7.6%, which is almost two times less than for the similar sample annealed at 1573 K (Table 1) and also shown by empty squares in Fig. 5 for convenience of comparison. It is clearly seen that an increase in the annealing temperature led to an increase in both the electrical conductivity and, accordingly, the power factor due to the better sintering of the sample, but at the same time had little effect on the Seebeck coefficient. This once again indicates that the behavior and magnitude of the Seebeck coefficient are largely determined by the intrinsic electronic structure, while the electrical conductivity and thermal conductivity significantly depend on the morphology and spatial organization of the material on the different scales.

4. Conclusions

The Sr_{1-x}Sm_xTiO₃ strontium titanate solid solutions were synthesized from oxides and carbonates by a conventional ceramic technology. The temperature dependences of the electrical conductivity and Seebeck coefficient of the samples with different doping levels ($x = 0.025, 0.05, 0.075, 0.1, \text{ and } 0.2$) were examined. The effect of mechanical activation, which leads to a decrease in the size of initial particles, was investigated. It was found that, with an increase in the samarium content from 0.025 to 0.075, the electrical conductivity increases and the absolute value of the Seebeck coefficient decreases, which improves the power factors of the samples with $x = 0.05$ and 0.075. The Seebeck coefficients at $x = 0.075, 0.1, \text{ and } 0.2$ are almost the same. The dependence of the electrical conductivity on the preliminary mechanochemical activation of the samples was established. It was demonstrated that the samples that were additionally mechanically activated have a significantly lower resistivity with only a minor change in the Seebeck coefficient. The best values of thermoelectric power factor were found for the samples formed by nanoparticles of the Sr_{0.95}Sm_{0.05}TiO₃ and Sr_{0.925}Sm_{0.075}TiO₃ compositions; these values are 5.5 μW/(cm · K²) at $T = 580$ K and 4.10 μW/(cm · K²) at $T = 650$ K, respectively. Thus, the level of samarium substitution in the range from 0.05 to 0.075 has the highest potential for improving the thermoelectric parameters of the Sr_{1-x}Sm_xTiO₃ samples and the additional mechanical activation allows one to improve the thermoelectric power factor and reduce the temperatures of sample synthesis and reduction. An increase in the annealing temperature of mechanically activated samples leads to an even greater increase in electrical conductivity and power factor: 9.2 μW/(cm · K²) for Sr_{0.925}Sm_{0.075}TiO₃ at $T = 650$ K.

Funding

This study was supported by the Russian Science Foundation, project no. 19-72-00097.

Declaration of competing interest

The authors declare that they have no known competing financial interests or personal relationships that could have appeared to influence the work reported in this paper.

Appendix A. Supplementary data

Supplementary data to this article can be found online at <https://doi.org/10.1016/j.ceramint.2021.07.060>.

References

- [1] Y.H. Lin, J. Lan, C. Nan, *Oxide Thermoelectric Materials*, Wiley-VCH, 2019.

- [2] A.F. Ioffe, *Termoelektrichestvo v poluprovodnikakh [Thermoelectricity in semiconductors]*, Zh. Tekhnicheskoy Fiz. 23 (1953) 1452–1455 (In Russian).
- [3] A.F. Ioffe, *Semiconductor Thermoelements and Thermo-Electric Cooling*, Infosearch Ltd, London, 1957.
- [4] H.J. Goldsmid, *Introduction to Thermoelectricity*, Springer, Berlin, 2010.
- [5] A.V. Kovalevsky, A.A. Yaremchenko, S. Populoh, P. Thiel, D.P. Fagg, A. Weidenkaff, J.R. Frade, Towards a high thermoelectric performance in rare-earth substituted SrTiO₃: effects provided by strongly-reducing sintering conditions, *Phys. Chem. Chem. Phys.* 16 (2014) 26946–26954, <https://doi.org/10.1039/C4CP04127E>.
- [6] K. Koumoto, Y. Wang, R. Zhang, A. Kosuga, R. Funahashi, Oxide thermoelectric materials: a nanostructuring approach, *Annu. Rev. Mater. Res.* 40 (2010) 363–394, <https://doi.org/10.1146/annurev-matsci-070909-104521>.
- [7] A. Mehdizadeh Dehkordi, S. Bhattacharya, T. Darroudi, J.W. Graff, U. Schwingschlögl, H.N. Alshareef, T.M. Tritt, Large thermoelectric power factor in Pr-doped SrTiO_{3-δ} ceramics via grain-boundary-induced mobility enhancement, *Chem. Mater.* 26 (2014) 2478–2485, <https://doi.org/10.1021/cm4040853>.
- [8] P.P. Shang, B.P. Zhang, J.F. Li, N. Ma, Effect of sintering temperature on thermoelectric properties of La-doped SrTiO₃ ceramics prepared by sol-gel process and spark plasma sintering, *Solid State Sci.* 12 (2010) 1341–1346, <https://doi.org/10.1016/j.solidstatesciences.2010.05.005>.
- [9] M. Ito, T. Matsuda, Thermoelectric properties of non-doped and Y-doped SrTiO₃ polycrystals synthesized by polymerized complex process and hot pressing, *J. Alloys Compd.* 477 (2009) 473–477, <https://doi.org/10.1016/j.jallcom.2008.10.031>.
- [10] J. Liu, C.L. Wang, W.B. Su, H.C. Wang, J.C. Li, J.L. Zhang, L.M. Mei, Thermoelectric properties of Sr_{1-x}Nd_xTiO₃ ceramics, *J. Alloys Compd.* 492 (2010) L54–L56, <https://doi.org/10.1016/j.jallcom.2009.11.165>.
- [11] A.V. Kovalevsky, A.A. Yaremchenko, S. Populoh, A. Weidenkaff, J.R. Frade, Enhancement of thermoelectric performance in strontium titanate by praseodymium substitution, *J. Appl. Phys.* 113 (2013), 053704, <https://doi.org/10.1063/1.4790307>.
- [12] T. Okuda, K. Nakanishi, S. Miyasaka, Y. Tokura, Large thermoelectric response of metallic perovskites: Sr_{1-x}La_xTiO₃ (0 < x < 0.1), *Phys. Rev. B* 63 (2001) 113104, <https://doi.org/10.1103/PhysRevB.63.113104>.
- [13] H. Muta, K. Kurosaki, S. Yamanaka, Thermoelectric properties of rare earth doped SrTiO₃, *J. Alloys Compd.* 350 (2003) 292–295, [https://doi.org/10.1016/S0925-8388\(02\)00972-6](https://doi.org/10.1016/S0925-8388(02)00972-6).
- [14] H.C. Wang, C.L. Wang, W.B. Su, J. Liu, Y. Zhao, H. Peng, J.L. Zhang, M.L. Zhao, J. C. Li, N. Yin, L.M. Mei, Enhancement of thermoelectric figure of merit by doping Dy in La_{0.1}Sr_{0.9}TiO₃ ceramic, *Mater. Res. Bull.* 45 (2010) 809–812, <https://doi.org/10.1016/j.materresbull.2010.03.018>.
- [15] C.S. Park, M.H. Hong, H.H. Cho, H.H. Park, Enhancement of Seebeck coefficient of mesoporous SrTiO₃ with V-group elements V, Nb, and Ta substituted for Ti, *J. Eur. Ceram. Soc.* 38 (2018) 125–130, <https://doi.org/10.1016/j.jeurceramsoc.2017.08.021>.
- [16] X. Li, H. Zhao, D. Luo, K. Huang, Electrical conductivity and stability of A-site deficient (La, Sc) co-doped SrTiO₃ mixed ionic-electronic conductor, *Mater. Lett.* 65 (2011) 2624–2627, <https://doi.org/10.1016/j.matlet.2011.05.109>.
- [17] Z. Lu, H. Zhang, W. Lei, D.C. Sinclair, I.M. Reaney, High-figure-of-merit thermoelectric La-doped A-site-deficient SrTiO₃ ceramics, *Chem. Mater.* 28 (2016) 925–935, <https://doi.org/10.1021/acs.chemmater.5b04616>.
- [18] J. Han, Q. Sun, Y. Song, Enhanced thermoelectric properties of La and Dy co-doped, Sr-deficient SrTiO₃ ceramics, *J. Alloys Compd.* 705 (2017) 22–27, <https://doi.org/10.1016/j.jallcom.2017.02.146>.
- [19] C. Chen, T. Zhang, R. Donelson, T.T. Tan, S. Li, Effects of yttrium substitution and oxygen deficiency on the crystal phase, microstructure, and thermoelectric properties of Sr_{1-x}Y_xTiO_{3-δ} (0 ≤ x ≤ 0.15), *J. Alloys Compd.* 629 (2015) 49–54, <https://doi.org/10.1016/j.jallcom.2014.12.125>.
- [20] J. Liu, C.L. Wang, Y. Li, W.B. Su, Y.H. Zhu, J.C. Li, L.M. Mei, Influence of rare earth doping on thermoelectric properties of SrTiO₃ ceramics, *J. Appl. Phys.* 114 (2013) 223714, <https://doi.org/10.1063/1.4847455>.
- [21] B. Poudel, Q. Hao, Y. Ma, X.Y. Lan, A. Minnich, B. Yu, X. Yan, D.Z. Wang, A. Muto, D. Vashaev, X.Y. Chen, J.M. Liu, M.S. Dresselhaus, G. Chen, Z.F. Ren, High-thermoelectric performance of nanostructured bismuth antimony telluride bulk alloys, *Science* 320 (2008) 634–638, <https://doi.org/10.1126/science.1156446>.
- [22] G.C. Dannangoda, C. Key, M. Sumets, K.S. Martirosyan, Transition of p- to n-type conductivity in mechanically activated bismuth telluride, *J. Electron. Mater.* 47 (2018) 5800–5809, <https://doi.org/10.1007/s11664-018-6469-1>.
- [23] Z. Lu, H. Zhang, W. Lei, D.C. Sinclair, I.M. Reaney, High-figure-of-merit thermoelectric La-doped A-site-deficient SrTiO₃ ceramics, *Chem. Mater.* 28 (2016) 925–935, <https://doi.org/10.1021/acs.chemmater.5b04616>.
- [24] L.A. Solovyov, Full-profile refinement by derivative difference minimization, *J. Appl. Crystallogr.* 37 (2004) 743–749, <https://doi.org/10.1107/S0021889805004899>.
- [25] A.T. Burkov, A. Heinrich, P.P. Konstantinov, T. Nakama, K. Yagasaki, Experimental set-up for thermopower and resistivity measurements at 100–1300 K, *Meas. Sci. Technol.* 12 (2001) 264–272, <https://doi.org/10.1088/0957-0233/12/3/304>.
- [26] A.T. Burkov, A.I. Fedotov, A.A. Kasyanov, R.I. Panteleev, T. Nakama, Methods and technique of thermopower and electrical conductivity measurements of thermoelectric materials at high temperatures, *Scientific and Technical Journal of Information Technologies, Mechanics and Optics* 15 (2015) 173–195, <https://doi.org/10.17586/2226-1494-2015-15-2-173-195>.
- [27] Z. Lu, H. Zhang, W. Lei, D.C. Sinclair, I.M. Reaney, High-Figure-of-Merit thermoelectric La-doped A-site-deficient SrTiO₃, *Ceramics Chemistry of Materials* 28 (2016) 925–935, <https://doi.org/10.1021/acs.chemmater.5b04616>.

- [28] R. Boston, W.L. Schmidt, G.D. Lewin, A.C. Iyasara, Z. Lu, H. Zhang, D.C. Sinclair, I. M. Reaney, Protocols for the fabrication, characterization, and optimization of n-type thermoelectric ceramic oxides, *Chem. Mater.* 29 (2017) 265–280, <https://doi.org/10.1021/acs.chemmater.6b03600>.
- [29] A. Kikuchi, N. Okinaka, T. Akiyama, A large thermoelectric figure of merit of La-doped SrTiO₃ prepared by combustion synthesis with post-spark plasma sintering, *Scripta Mater.* 63 (2010) 407–410, <https://doi.org/10.1016/j.scriptamat.2010.04.041>.
- [30] K. Park, J.S. Son, S.I. Woo, K. Shin, M.-W. Oh, S.-D. Park, T. Hyeon, Colloidal synthesis and thermoelectric properties of La-doped SrTiO₃ nanoparticles, *J. Mater. Chem.* 2 (2014) 4217–4224, <https://doi.org/10.1039/C3TA14699E>.
- [31] M. Qin, F. Gao, G. Dong, J. Xu, M. Fu, Y. Wang, M. Reece, H. Yan, Microstructure characterization and thermoelectric properties of Sr_{0.9}La_{0.1}TiO₃ ceramics with nano-sized Ag as additive, *J. Alloys Compd.* 762 (2018) 80–89, <https://doi.org/10.1016/j.jallcom.2018.05.202>.
- [32] Al Jumlat Ahmed, Sheik Md Kazi Nazrul Islam, Ridwone Hossain, Jeonghun Kim, Minjun Kim, Motasim Billah, Md Shahriar A. Hossain, Yusuke Yamauchi, Xiaolin Wang, Enhancement of thermoelectric properties of La-doped SrTiO₃ bulk by introducing nanoscale porosity, *R. Soc. open sci.* 6 (1–9) (2019) 190870, <https://doi.org/10.1098/rsos.190870>.
- [33] Xiao-Lei Shi, Hao Wu, Qingfeng Liu, Wei Zhou, Siyu Lu, Zongping Shao, Matthew Dargusch, Zhi-Gang Chen, SrTiO₃-based thermoelectrics: progress and challenges, *Nanomater. Energy* 78 (2020) 105195, <https://doi.org/10.1016/j.nanoen.2020.105195>.